◇ Monograph Excerpt ◇

Matter Antimatter Fluctuations

search, discovery and analysis of Bs flavor oscillations

Nuno Leonardo

Complete work published as:
Analysis of B_s oscillations at CDF, MIT Thesis (2006)
Matter antimatter fluctuations, Monograph, LAP Lambert (2011)

Amplitude scanning and validation

.4 Fitting framework validation

The unbinned maximum likelihood fit is of considerable complexity. In the development of the fitting framework, the starting point is provided by simplified models. Successive complications are then progressively introduced. The $J/\psi K$ samples were particularly useful at many stages in this respect. Their sample composition, mass and proper time models happen to be relatively simpler in general. When deriving the implementation of trigger bias in the proper decay time distribution, it was insightful again to work with the unbiased $J/\psi K$ samples. Biases were introduced as ad-hoc selection thresholds, such as simple, direct cuts on proper time. It became apparent, using actual data in this way, that certain approaches previously attempted do not suit. Once solutions for the simpler cases are found, further elaborations alongside similar lines are then pursued.

A technique that was consistently employed in the development of the fitting model and for checking implementation consistency was that of toy Monte Carlo. Events are sampled according to the likelihood model. If a large enough number of events is generated, its distribution will exactly coincide, by design, with the likelihood function. In these circumstances, a fit to the data should return precisely the parameter values that were employed for the generation. This is a useful consistency test. Differences between the expected value parameter and its value returned by the fit must be due to statistical fluctuations. The distribution of such differences, referred to as "pull", should be consistent with a unit Gaussian centered at zero. To achieve the proper statistical fluctuation, the number of events simulated for each sample is matched to that collected in the data. This allows a direct, quantitative determination of whether the values returned by the likelihood are unbiased estimators of the fit parameters. A selection of pull distributions is shown in Figure 1. The Gaussian characteristics of such distributions for selected parameters are shown in Tables 1 – 3.

parameter	mean	width	Gaussian fit prob.
M	0.025 ± 0.023	1.043 ± 0.017	0.937
σ_m	-0.036 ± 0.023	1.027 ± 0.016	0.786
f_{bg}	-0.012 ± 0.022	0.993 ± 0.016	0.787
$c\tau$	-0.025 ± 0.022	1.004 ± 0.016	0.231
backgr. $c\tau$	-0.049 ± 0.023	1.014 ± 0.016	0.228
backgr. offset	0.009 ± 0.022	0.999 ± 0.016	0.742
backgr. σ	-0.106 ± 0.023	1.026 ± 0.016	0.219

Table 1: Characteristics of pull distributions for mass and lifetime fits; 1000 events per pseudo-experiment.

parameter	mean	width	Gaussian fit prob.
m	0.088 ± 0.031	0.987 ± 0.022	0.969
$c\tau$	-0.021 ± 0.033	1.029 ± 0.023	0.884
Δm_d	0.012 ± 0.033	1.047 ± 0.023	0.032
SMT ϵ	-0.064 ± 0.031	0.981 ± 0.022	0.780
JJP ϵ	-0.011 ± 0.031	0.988 ± 0.022	0.459
SMT $\mathcal{D}$	0.092 ± 0.031	0.994 ± 0.022	0.782
JJP $\mathcal{D}$	-0.002 ± 0.033	1.049 ± 0.023	0.985
SMT ϵ_{bg}	-0.029 ± 0.031	0.991 ± 0.022	0.950
JJP ϵ_{bg}	0.046 ± 0.031	0.970 ± 0.022	0.781
SMT $\mathcal{D}_{bg}$	-0.016 ± 0.032	1.017 ± 0.023	0.013
JJP $\mathcal{D}_{bg}$	0.018 ± 0.032	1.011 ± 0.023	0.554

Table 2: Characteristics of pull distributions for mixing fits; 2000 events per pseudo-experiment, two taggers, $\Delta m = 0.5$ ps^{-1}.

parameter	mean	width	Gaussian fit prob.
m	0.034 ± 0.033	1.054 ± 0.024	0.610
$c\tau$	-0.055 ± 0.032	1.012 ± 0.023	0.389
$\mathcal{A}$	-0.007 ± 0.034	1.062 ± 0.024	0.662
SMT ϵ	-0.076 ± 0.033	1.042 ± 0.023	0.245
JJP ϵ	-0.052 ± 0.032	1.018 ± 0.023	0.235
SMT ϵ_{bg}	-0.028 ± 0.032	0.998 ± 0.022	0.568
JJP ϵ_{bg}	-0.005 ± 0.032	1.010 ± 0.023	0.827
SMT $\mathcal{D}_{bg}$	-0.034 ± 0.033	1.046 ± 0.023	0.697
JJP $\mathcal{D}_{bg}$	0.024 ± 0.032	1.022 ± 0.023	0.373

Table 3: Characteristics of pull distributions for amplitude scan fits; 2000 events per pseudo-experiment, two taggers with fixed dilution scale factors, $\Delta m = 15$ps^{-1}.

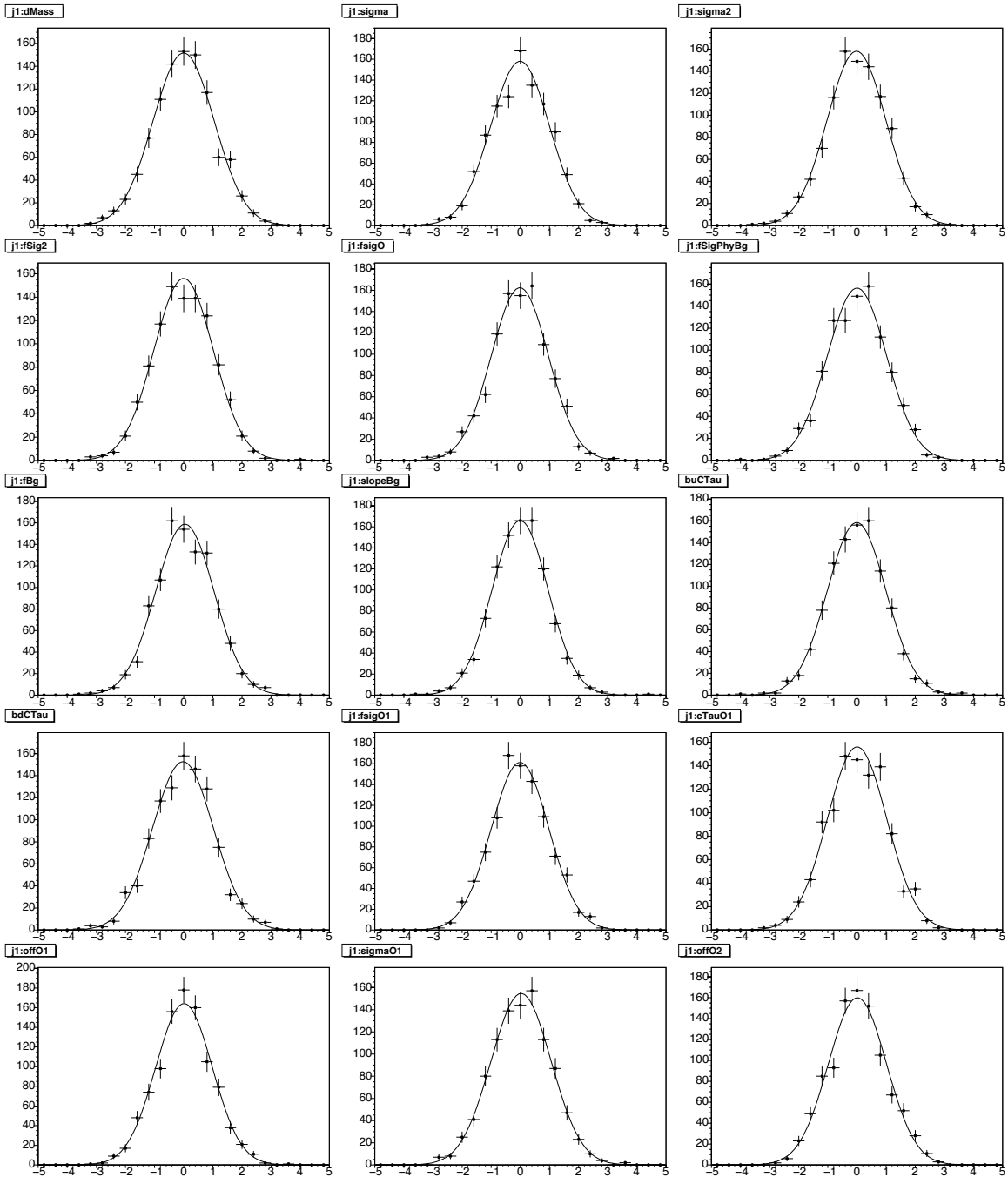

Figure 1: Toy Monte Carlo pull distributions, for a selection of mass and proper time fit parameters.

.5 Shape of the amplitude scan profile

In the amplitude scan method, in case the probe frequency coincides with that of the oscillating system, the amplitude is expected to be maximal and unity. As frequencies away from that true value are probed, the amplitude is expected to approach zero. The shape of the resonance peak is expected to be given, modulo slowly varying functions, by a Breit-Wigner function, whose width is determined by the lifetime of the system. This issue is investigated using Fourier analysis, as is done in Section 11.1. In case, however, the proper decay time distribution is biased, deviating from the form of a smeared exponential, so-called *undershooting* effects are expected on both sides of the amplitude peak.

The appearance of such effects has been demonstrated for the case of a simple bias in (11.13). A graphical representation is provided in Figure 2. This is a simple, convenient illustration of the origin behind the general effect. A more elaborate analytical treatment may be pursued to account for more realistic conditions. However, for such more complex, specific cases a simulation of the involved sample characteristics becomes appropriate. The scan obtained from a full fit of a toy Monte Carlo mixing sample is shown in Figure 3, for a representative frequency of Δm_d. The generation of the sample is performed both including and excluding the characteristic proper time bias, using in the fit model the t-efficiency function and turning it off, as appropriate. The undershooting is verified in the former case and absent in the latter, as expected. The amplitude scan performed on an actual *data* sample of fully reconstructed B^0 decays is shown in Figure 4(a) [61].

We make now a worthy consideration about the width of the amplitude peak. As it is apparent from Figures 2 and 3, as well as from (11.13), the biasing of the proper time distribution induces a narrowing of the peak relative to the unbiased case. In this latter case, the width is determined essentially by the lifetime τ of the system. However, the same effect which, in the t-biased case, is responsible for the undershooting, also induces the width narrowing. This translates in turn into a narrowing of the likelihood profile for Δm (which corresponds to the logarithm of the likelihood ratio in (12.28)) and ultimately in a decrease of the uncertainty in the Δm determination. By preferentially selecting B events further displaced from the production point, samples with larger proper decay times are formed, which more precisely probe the frequency of the oscillations.

The oscillating undershooting pattern is visible near the B_s frequency peak in Figure 4(b) for the combined scan of the first Δm_s measurement [100], and no less prominently in the decay-mode specific scans of Figures 10.7 and 10.8 yielding the observation of B_s oscillations [101]. As demonstrated, these are as expected, from the characteristics of the proper time distributions induced by the trigger and selection criteria employed to collect the data.

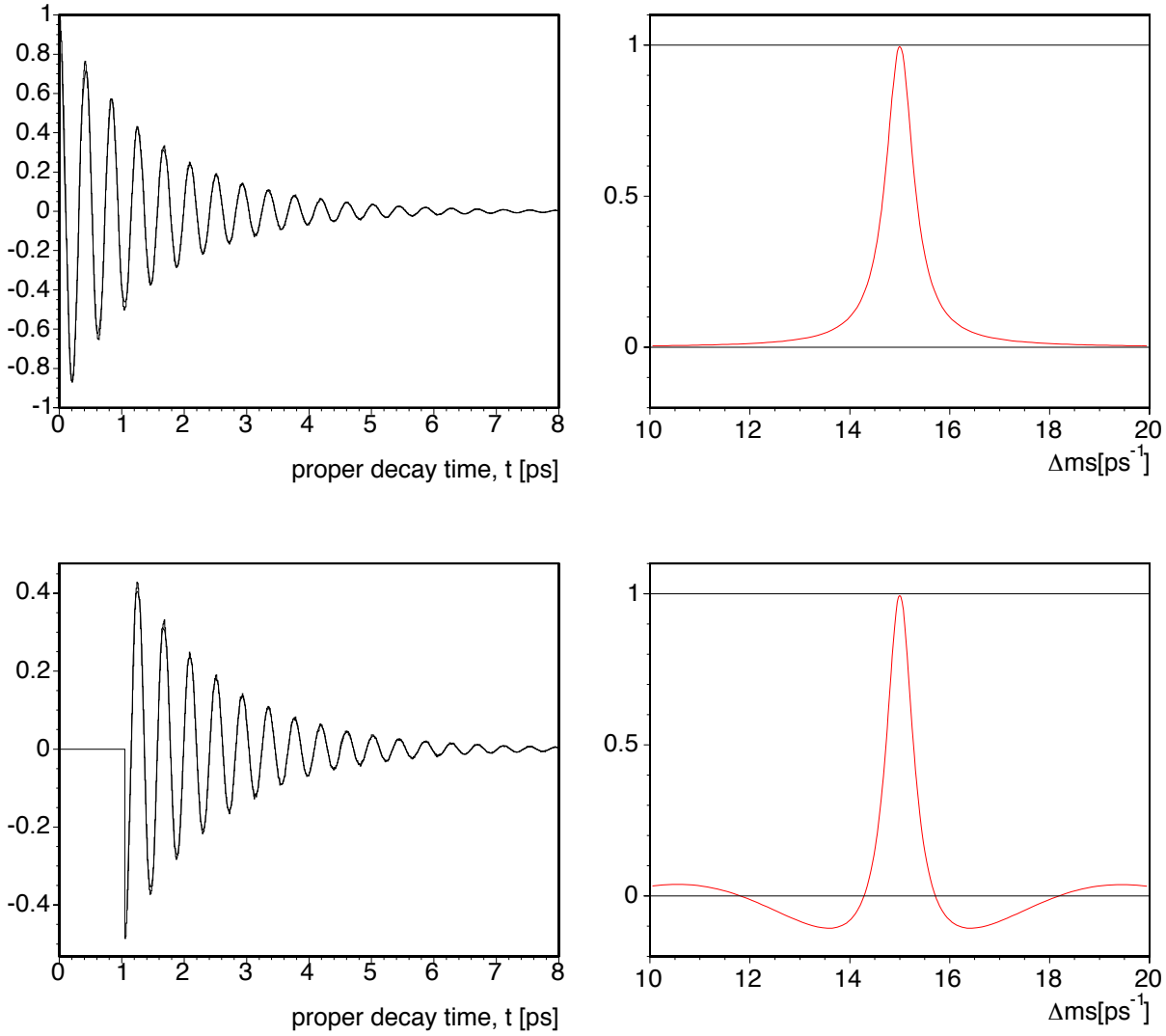

Figure 2: Illustration of the amplitude scan shape for the case of unbiased proper decay time (top) and in the presence of a direct cut (bottom); the graphs on the left indicate the asymmetry distributions, while those on the right represent the corresponding Fourier transforms.

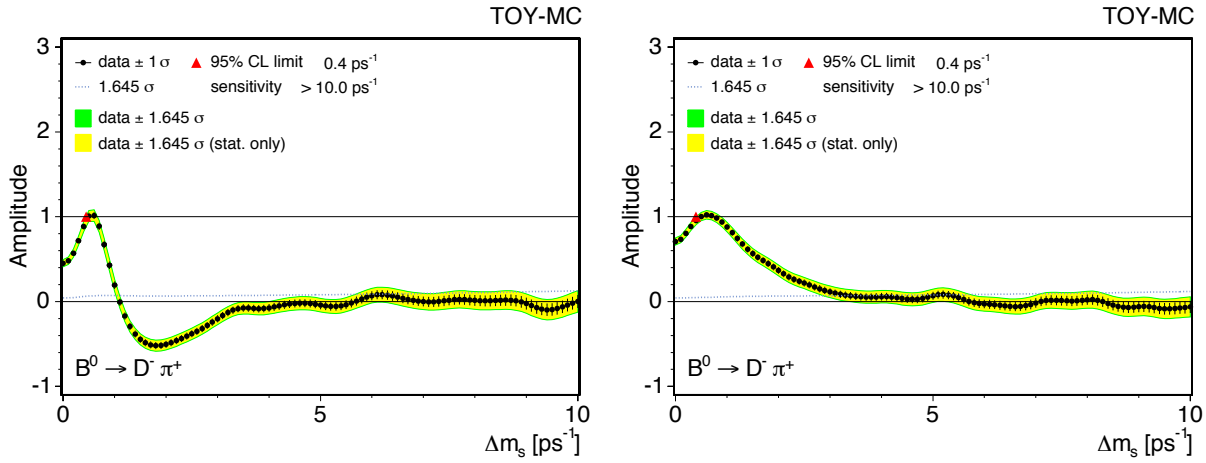

Figure 3: Illustration of t-biasing effects on the amplitude scan, using realistic toy simulation for the Δm_d case: (left) with biased t distribution, and (right) for the unbiased case where the efficiency function was been disabled.

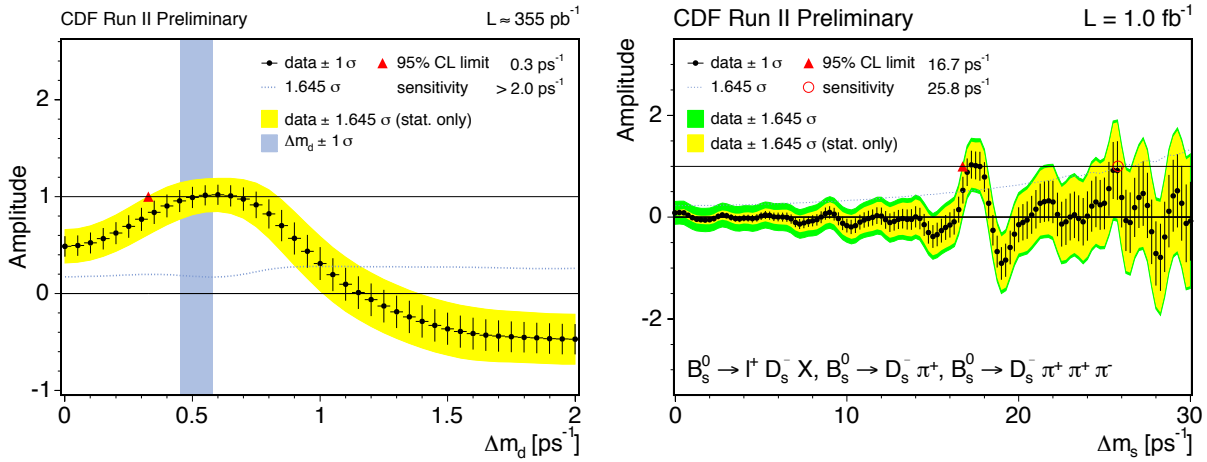

(a) B^0 oscillation scan.

(b) B_s oscillation scan.

Figure 4: Amplitude scan performed on data, for the B^0 (left) and B_s (right), displaying expected undershooting in the vicinity of the peaks.